DFT calculations of carrier-trapping effects on atomic structures of 30° partial dislocation cores in zincblende II-VI group zinc compounds

Sena Hoshino,[1,*] Yu Oshima,[1] Tatsuya Yokoi,[1] Atsutomo Nakamura,[2] and Katsuyuki Matsunaga[1,3,†]
[1]*Department of Materials Physics, Nagoya University, Furo-cho, Chikusa, Nagoya 464-8603, Japan*
[2]*Department of Mechanical Science and Bioengineering, Osaka University, 1-3 Machikaneyama-cho, Toyonaka, Osaka 560-8531, Japan*
[3]*Nanostructures Research Laboratory, Japan Fine Ceramics Center, 2-4-1 Mutsuno, Atsuta, Nagoya 456-8587, Japan*

(Received 5 October 2022; revised 20 December 2022; accepted 4 January 2023; published 17 January 2023)

It was experimentally reported that II-VI group inorganic semiconductor crystals become harder and brittle by external light illumination. In order to reveal essential factors of the light illumination effect, systematic GGA + U calculations are performed for 30° partial dislocations in ZnSe and ZnTe, and the obtained results are discussed together with those for ZnS reported previously. It is found in these three crystal systems that the cores of pristine partial dislocations have unreconstructed atomic structures whereas their cores undergo atomic reconstruction energetically more favorably by trapping excess carriers. Such carrier trapping and atomic reconstruction of the dislocation cores are ascribed to the presence of excess electrostatic potentials at the cores due to ionic bonding characters of the host crystals. The dislocation core reconstructions decrease potential energies of the partial dislocations and can in turn increase Peierls-potential barriers for dislocation glide, corresponding to the observed hardening and brittleness by light illumination. The energy gains due to the dislocation-core reconstructions also depend on energy positions of the defect-induced levels that appear within the band gaps.

DOI: 10.1103/PhysRevMaterials.7.013603

I. INTRODUCTION

Inorganic II-VI group semiconductors meet many applications such as optical devices, solar cells, and light-emitting diodes, because of their excellent electronic and optical properties. One disadvantage of those materials is limited processability as they are typically brittle at room temperature and easily fracture even by small external forces. With recent development in nanostructures and three-dimensional (3D) structures for electronic devices, there is an urgent need to improve processability and reliability of semiconductors. It is thus essential to gain a deeper understanding of their mechanical properties and to ultimately find efficient ways to control them.

One of the fascinating phenomena in the mechanical behavior of semiconductors is the photoplastic effect (PPE). The PPE was typically observed for II-VI semiconductors such as Zn or Cd compounds [1–3], where their deformation stresses increase by light illumination, indicating hardening of the crystals. In contrast, our research group discovered that ZnS single crystals show extraordinary plasticity in complete darkness whereas they show brittleness under light illumination [4,5], demonstrating that brittleness and ductility of ZnS can be switched by controlling light environments. Since generation and multiplication of glide dislocations are responsible for the observed plasticity of ZnS in darkness, it can be speculated that the PPE of ZnS is due to changes of glide dislocation mobility by external light, to be more specific, reduced dislocation mobility under light illumination [6].

Regarding a mechanism of the PPE, it is essential to reveal how light illumination can influence glide dislocation mobility. Our density-functional theory (DFT) calculations on ZnS indicated that Shockley partial dislocations in ZnS formed by applied stresses can trap excess electrons and holes at around the dislocation cores [7]. When ZnS is irradiated by UV light, electrons and holes are excited via interband transitions. Because ZnS has relatively strong ionicity, the dislocations can develop an electrostatic field at their cores locally, and as a result, the photoexcited carriers tend to be trapped at dislocations. It was also found that the partial dislocations undergo atomic reconstructions at the cores only when they trap excess carriers. It is worth mentioning that the core reconstructions can be attained by formation of like-atom bonds of Zn-Zn or S-S at the cores. Such carrier trapping and the resultant atomic reconstructions at the dislocation cores make the partial dislocations energetically more stable, as compared to those without carrier trapping. When the partial dislocations are about to glide, such like-atom bonds of the reconstructed cores have to be broken, which should retard the dislocation mobility. These results strongly claim the importance of the partial-dislocation structures on the PPE-related mechanical behavior [5].

As stated above, the electrostatic fields and formation of like-atom bonds at the dislocation cores should be responsible for the PPE in ZnS. Since these originate from relatively strong ionicity of ZnS, original electronic structures of host inorganic semiconductors may be critical for the PPE. In fact, the PPE of some semiconductors such as Si is known to be different from that of the II-VI semiconductors [8–11]. However, it still remains open as to what inorganic semiconductors can exhibit PPE and how PPE differs from semiconductor to

*hoshino.sena.i9@s.mail.nagoya-u.ac.jp
†kmatsunaga@nagoya-u.jp

semiconductor. To this end, it is necessary to conduct systematic studies on the electronic and atomic structures of glide dislocations in inorganic semiconductors. In this study, a series of II-VI group zinc compounds having the zincblende structure (ZnS, ZnSe, and ZnTe) are selected, and DFT calculations are performed to investigate their most stable atomic structures and energetics of the partial dislocations with and without extra carriers. From electrostatic potential fields and local densities of states (LDOSs) at the partial dislocations, potential carrier trapping at the partial dislocation cores is examined. Formation energies of the partial dislocations are evaluated to clarify whether atomic reconstruction at the dislocation cores takes place in the presence of excess carriers. Along with the results for ZnS in our previous paper [7], differences in reconstruction energies at the dislocation cores of ZnS, ZnSe, and ZnTe are discussed.

II. COMPUTATIONAL METHOD

A. DFT calculation

DFT calculations were performed with the projector augmented wave (PAW) method implemented in the VASP code [12,13]. The exchange-correlation functional within the generalized gradient approximation (GGA) parameterized by Perdew, Burke, and Ernzerhof (PBE) was used [14]. In the PAW potential, 3*d* and 4*s* orbitals for Zn, 4*s* and 4*p* orbitals for Se, and 5*s* and 5*p* orbitals for Te were treated as valence electrons. Cutoff energies of plane waves were set at 400 eV. For Brillouin zone integration, $1 \times 2 \times 6$ and $1 \times 2 \times 3$ k-point meshes were used for 288- and 576-atom supercells, respectively. Details of the supercells are described below. In addition, different-sized supercells were used to investigate the supercell-size effects, where their k-point meshes were determined so as to have the comparable k-point densities. The GGA + U method was used to correct on-site Coulomb repulsion since typical GGA functionals are known to fail to properly describe localization of d electrons [15]. The effective U parameters were empirically chosen to be 8 for the Zn-3*d* orbitals, so as to reproduce measured values of their energy levels [16]. It is noted that a similar U value was often used for point defects and amorphous structures in Zn compounds [17–19]. Theoretical band gaps obtained using the GGA + U method were as follows: 1.94 eV for ZnSe and 1.73 eV for ZnTe. These values are smaller than the experimental values (2.7 eV for ZnSe and 2.25 eV for ZnTe [20]). For structural relaxation, atomic positions were updated until forces acting on atoms became smaller than 0.01 eV/Å. Since the same computational conditions were used even for ZnS in our previous paper [7], the results in ZnS were also discussed along with those in ZnSe and ZnTe.

B. Dislocation modeling

As a typical glide dislocation in the zincblende II-VI zinc compounds, the present study modeled 30° partial dislocations with a Burgers vector of 1/6 $\langle\bar{2}11\rangle$, according to the following reason. For the zincblende crystals, the primary slip system is generally considered as the $\langle\bar{1}10\rangle$ direction on the {111} plane at room temperature. It was reported that the glide dislocations introduced in ZnS are not perfect dislocations but pairs of partials having the Burgers vector of 1/6 $\langle\bar{2}11\rangle$ with a stacking fault on {111} [7]. When a dislocation loop on {111} is invoked in the zincblende structure, the loop is dissociated with the partials, and segments of the dissociated loop are composed of 30° −30° and 30° −90° partial dislocation pairs. Owing to the requirement of the periodic boundary conditions of the present DFT calculations, a pair of 30° −30° partial dislocations was considered. This is also reasonable from the aspect of self-energies of dislocations, because self-energies of dislocations generally tend to be smaller with increasing their screw components of the Burgers vectors (namely, 30° partials are more stable than 90° partials).

TABLE I. Calculated stacking fault energies (SFEs) and stacking faults widths d_{SF}. The corresponding experimental stacking fault energies are also listed [21].

	DFT		Expt.[a]
	SFEs (mJ/m^2)	d_{SF} (nm)	SFEs (mJ/m^2)
ZnS	8[b]	41[b]	$\leqslant 6$
ZnSe	18	21	13 ± 1
ZnTe	18	15	16 ± 2

[a]Reference [21].
[b]Reference [25].

Similar to the case in ZnS, the presence of the partial dislocation pairs was experimentally observed in other II-VI semiconductors [21–24]. To theoretically confirm them, possibilities of the dissociated partial dislocation pairs in the II-VI zinc compounds were investigated on the basis of the elastic theory. This was done in the way that stacking fault energies (SFEs) on {111} planes were evaluated by DFT calculations and equilibrium distances between the 30° partials were obtained from balances between repulsive elastic forces of the two partials and attractive forces due to extension of SFEs (for detailed calculation see [25]). The elastic force between two partial dislocations (i and j) f_{ij} were calculated from the Peach-Koehler's equation as follows [26]:

$$f_{ij} = \frac{G}{2\pi}\left(\frac{b_i^e b_j^e}{1-\nu} - b_i^s b_j^s\right)\frac{1}{d_{SF}}. \quad (1)$$

G and ν are the shear modulus and the Poisson's ratio, and the following values calculated in our group were used here: 33.8 GPa and 0.26 for ZnS [25], 33.8 GPa and 0.27 for ZnSe, 25.7 GPa and 0.27 for ZnTe. b^e and b^s are the absolute values of the edge and screw components of the partial dislocations.

The results obtained are summarized in Table I. The calculated SFEs were in good agreement with experimentally reported values, and the resultant estimated equilibrium widths of the partial dislocations (d_{SF}) were more than 10 nm. This also ensures that the present computational conditions support dissociation of the glide dislocations into Shockley partials in these II-VI zinc compounds as observed experimentally.

To model 30° partial dislocations, the following two points should be considered. The first point is off-stoichiometry of the partial dislocation cores. Because {111} slip planes for the zincblende structure are polar planes, 30° partial dislocations have excess cations or anions at the cores, which are referred

to as the cation and anion cores, respectively, in the present study; in the standard electronic structure calculations, the term "core" often means core orbitals in contrast to valence orbitals whereas the present study mainly uses it as a meaning of the central atomic structures of the dislocations. Owing to three-dimensional periodic boundary conditions, each dislocation supercell has to contain a pair of partial dislocations having a cation core and an anion core with a stacking fault on {111}, for which the sum of their Burgers vectors is zero within each entire supercell. In the present dislocation supercells, these dislocations were located at quadrupole positions over the image supercells to cancel elastic forces between the dislocations. In the supercell calculations of the partial dislocation pairs, basically, a stacking-fault width between the partials (d_{SF}) was set at 2.8 nm. Then the total number of atoms in the supercells mainly used in the present study was 288.

It is noted here that some of previous DFT calculations of dislocations used the cluster models passivated by pseudohydrogen atoms at the surfaces. However, our test calculations showed that the cluster model of a partial dislocation induces artificial electrostatic fields at the surface atoms (see Fig. S1 of the Supplemental Material [27]). The periodic supercell models used in the present study are more adequate because they can avoid such artificial electrostatic fields.

The second point considered here is a possibility of core reconstruction. Previous theoretical studies indicated that reconstructed double-period (DP) structures of 30° partial dislocations are more stable in some semiconductor crystals than their unreconstructed structures (see also Fig. 3 shown later) [28–34]. For DP structures, new like-ion bonds are formed to eliminate dangling bonds at the unreconstructed cores, which were considered in the present study. It is noted that a DP core has double periodicity along its dislocation line, as compared to an unreconstructed core, so that the supercells were obtained by doubling the 288-atom supercells along the dislocation lines (576-atom supercells).

C. Supercell size dependence

The d_{SF} value in the above-mentioned supercell size (288 or 576 atoms) is much smaller than experimental observed or theoretically predicted data (see Table I). As will be discussed later (e.g., Fig. 4), the partial dislocations have excess electrostatic potentials localized at their cores due to off-stoichiometry and ionicity in the chemical bonds. Therefore, electronic structures around the partial-dislocation cores may also be subjected to the supercell-size dependence. In order to address this issue, test calculations using different sized supercells for the partial-dislocation pair in ZnSe were made.

Figure 1(a) shows LDOS profiles at the cation and anion cores in ZnSe for different sized supercells. Here, the partial dislocations have unreconstructed atomic structures at their cores [see Figs. 3(a) and 3(b)], and the LDOS profiles were obtained for the atoms at the respective cores, marked in Figs. 3(a) and 3(b)]. In addition to the 288-atom supercell ($d_{SF} = 2.8$ nm), 48-atom ($d_{SF} = 1.4$ nm), 144-atom ($d_{SF} = 2.1$ nm), and 480-atom ($d_{SF} = 3.5$ nm) supercells were used here. It can be seen that valence band maximums (VBMs) at the anion cores are higher in energy than the VBM in bulk

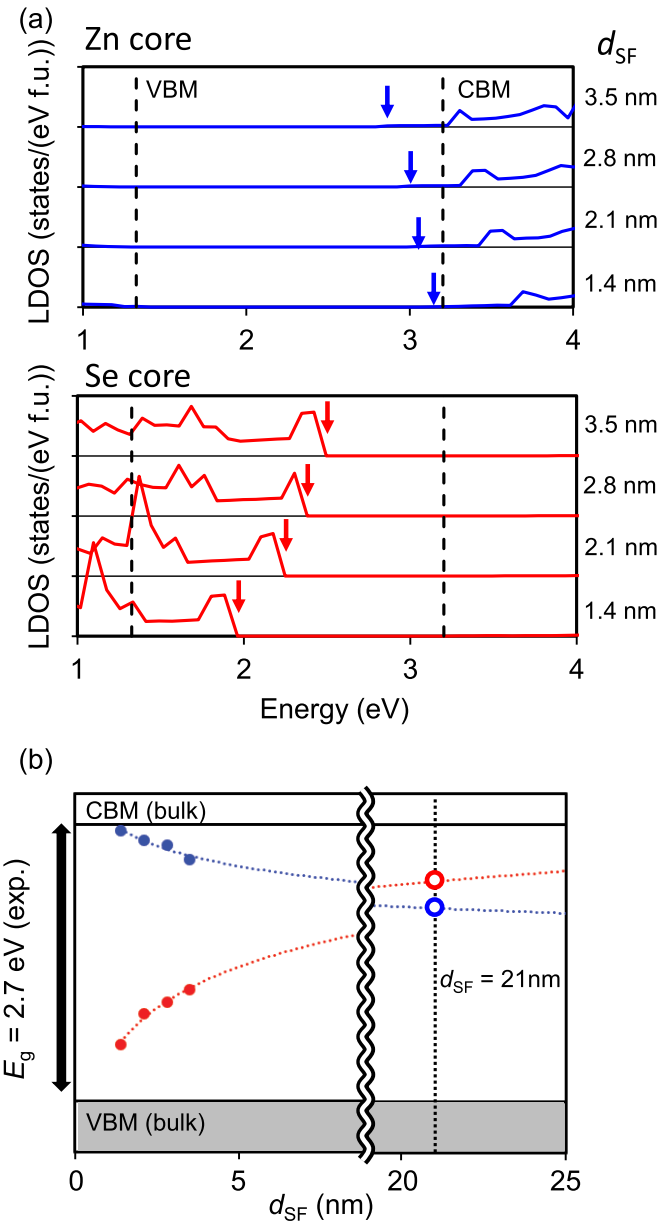

FIG. 1. (a) LDOS curves at the cation core and anion core in ZnSe with different stacking fault widths (1.4, 2.1, 2.8, and 3.5 nm). These are taken only from the central atoms at the dislocation cores and their nearest neighbors. The VBM and CBM in bulk are indicated by vertical dashed lines. (b) VBM and CBM positions at the anion and cation cores in the supercells plotted against stacking-fault width (d_{SF}). The red and blue dot curves are fitted VBM and CBM positions of the anion and cation cores for larger d_{SF}, respectively.

while conduction band minimums (CBMs) at the cation cores are lower in energy than the CBM in bulk. These are so-called defect induced states localized at the partial-dislocation cores. The VBM positions at the anion cores (CBM positions at the cation cores) in the LDOS profiles tend to shift higher (lower) in energy with increasing d_{SF}. However, within these supercell sizes, the VBM and CBM positions at the partial-dislocation cores are energetically separated from each other within the band gap. This corresponds to the situation in Fig. 2(a), where the valence bands of the LDOS profiles are usually fully

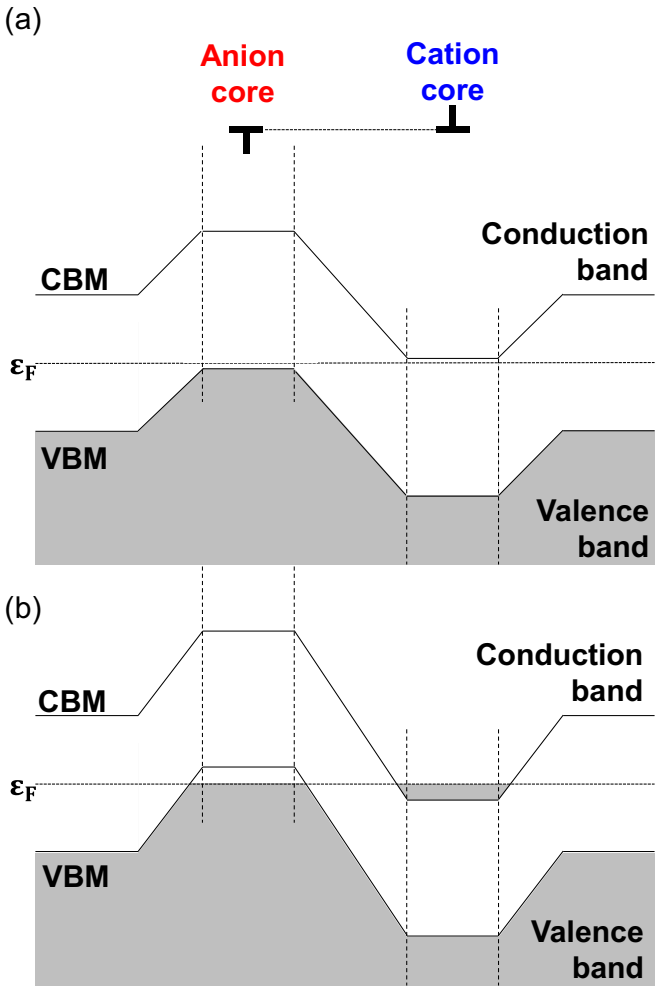

FIG. 2. Schematic band structures of the 30° partial-dislocation pair in (a) the fully ionized states and (b) the partially ionized states. The gray areas mean energy levels occupied by electrons.

occupied, irrespective of the supercell sizes. This means that atoms at the partial-dislocation cores are in the fully ionized states.

Such changes in VBM and CBM positions depending on the supercell sizes can be qualitatively understood from an electrostatic model of an infinite line of charge. The partial dislocations in the supercells are parallel to each other at a distance of d_{SF}, and then the dislocation lines are regarded as infinite lines with a uniform charge density of Q ($Q > 0$ at the cation core and $Q < 0$ at the anion core). An electric field E of the line charge (normal to the line) at a perpendicular distance r is expressed as

$$E = Q/2\pi\varepsilon r. \tag{2}$$

ε is a permittivity of a substance. An electron at the position r has a potential energy U as

$$U = \frac{eQ}{2\pi\varepsilon}\ln(r) + U_0, \tag{3}$$

where e is the elementary charge and U_0 is a constant. On the basis of this model, it is assumed that electrons at the VBM of the anion core (at the CBM of the cation core) are subjected to the electric field of the cation core with $Q > 0$ (anion core with $Q < 0$) at a distance of d_{SF}. According to Eq. (3), VBM positions at the anion core should increase in energy with rising d_{SF} as $\ln(d_{SF})$ while CBM positions at the cation cores should decrease.

At large d_{SF} as found in Table I, the VBM position at the anion core and the CBM position at the cation core likely come close to each other in energy, which may happen to bring about charge transfer between the cores. Since it was very demanding to calculate supercells with realistic d_{SF}, the VBM and CBM positions at the anion and cation cores in the supercells were fitted with $\ln(d_{SF})$ to predict them at large d_{SF} by extrapolation [see Fig. 1(b)]. In the figure, the experimental band gap (2.7 eV) was used because DFT calculations underestimate the band-gap value (1.94 eV). Extrapolation to a realistic $d_{SF} = 21$ nm (see Table I) indicates that the VBM of the anion core becomes slightly higher in energy (by 0.26 eV) than the CBM of the cation core. This may correspond to the situation illustrated in Fig. 2(b). Energy levels at the VBM of the anion core and the CBM of the cation core may be partially filled at the large d_{SF}, which is a different picture from the fully ionized states as Fig. 2(a) [see also Fig. 1(a)]. However, the above extrapolation does not consider electronic relaxation and thus equilibration of the Fermi levels in bulk and at the dislocation cores. It is expected that equilibration of the Fermi levels ends up with the picture close to Fig. 2(a), indicating quite small charge transfer between the cation and anion cores. This is because larger charge transfer between dislocation cores reduces ionic charges of constituent atoms at the dislocation cores and should be energetically much less stable in the ionically bonded crystals. Therefore, it is reasonable to approximate that the cation and anion cores in ZnSe are also in the almost fully ionized states. It is confirmed that such a situation is indeed realized in the present 288-atom supercells (see also Fig. 5 shown later).

D. Dislocation formation energy

In order to investigate stability of the partial dislocations with or without excess carriers, their formation energies as a function of excess charge q, $\Delta E_f(q)$, were calculated. The value of q was assumed to take an integer and to be varied in the range between -4 and $+4$. $q = 0$ means the neutral supercell (the pristine supercell). $\Delta E_f(q)$ was calculated by

$$\Delta E_f(q) = E_T(\text{dislocation},\ q) - E_T(\text{perfect}) + q(E_{VBM} + \varepsilon_F), \tag{4}$$

where $E_T(\text{dislocation},\ q)$ and $E_T(\text{perfect})$ are total energies of the dislocation supercell with q and the perfect-crystal supercell, respectively. E_{VBM} is the VBM energy in bulk, and ε_F is the Fermi energy with respect to the VBM. Since E_{VBM} of the dislocation supercells may be different from that of the perfect supercell, E_{VBM} values of the dislocation supercells were corrected by average electrostatic potentials as [35]

$$E_{VBM} = E_{VBM}^{perfect} + V_{av}^{disloc} - V_{av}^{perfect}, \tag{5}$$

where V_{av}^{disloc} and $V_{av}^{perfect}$ are average potentials in the bulklike regions (away from the partial dislocations) in the supercells. $E_{VBM}^{perfect}$ was obtained from a total energy of the neutral perfect

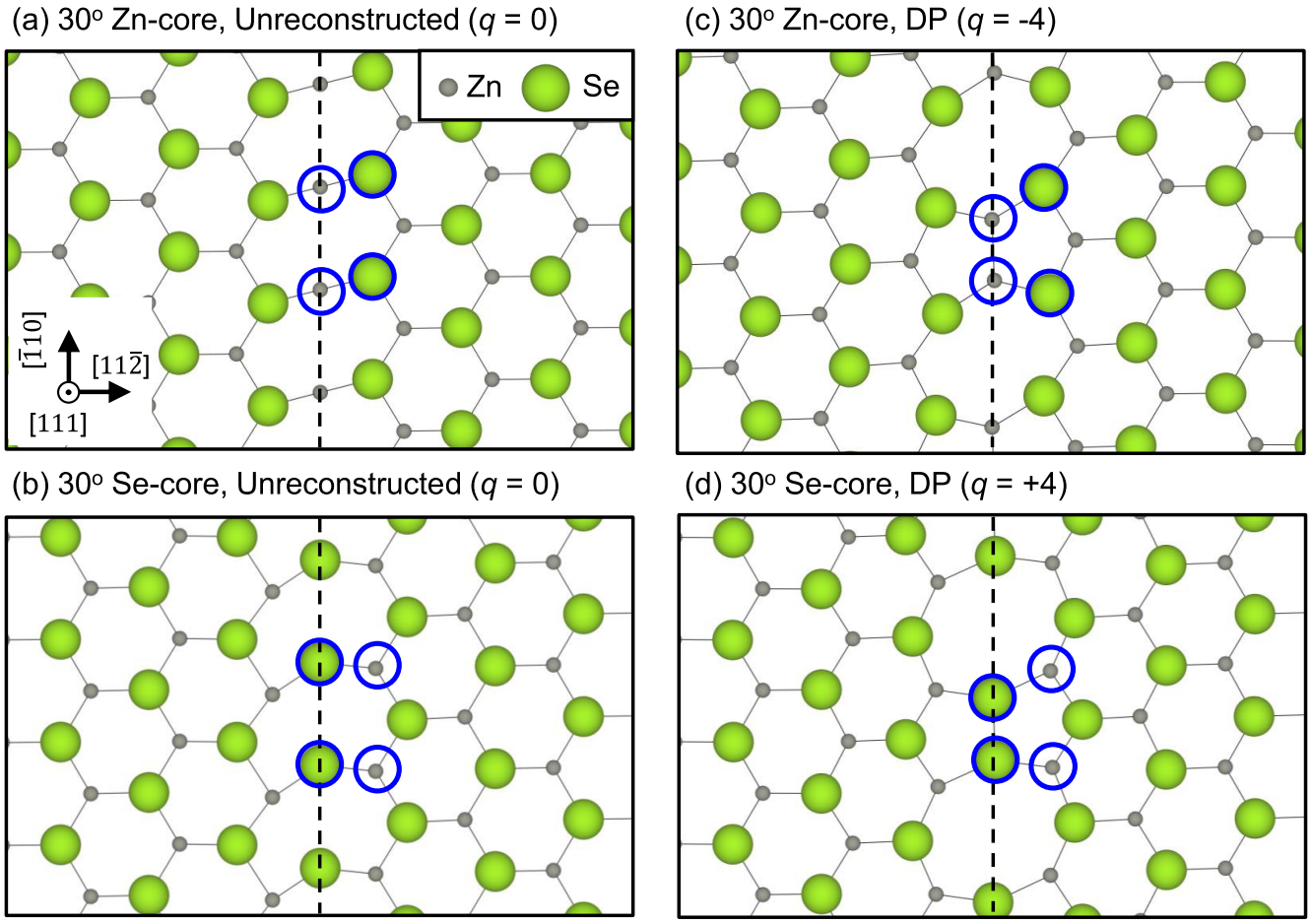

FIG. 3. Calculated most stable atomic structures of the 30° partials at the Zn and Se cores with $q = 0$ and ± 4 in ZnSe. These are viewed normal to the slip planes of {111}. The dashed lines correspond to the dislocation lines. The gray and light green balls represent Zn and Se atoms, respectively. Atoms circled indicate the ones used for LDOS analyses.

supercell minus that of the perfect supercell from which one electron was removed.

It is known that finite-sized supercells for charged defects involve spurious electrostatic interactions with their images in the periodic boundary conditions [36]. Then, E_{T} (dislocation, q) converges as L^{-1}, where L is a dimension of the supercell. E_{T} (dislocation, q) without the spurious interactions is thus obtained in the limit $L \to \infty$. In order to make the corrections in the present formation-energy evaluations, additional different-sized supercells (48 and 144 atoms) were used. In the present case, it is noted that L corresponds to supercell dimensions normal to the dislocation lines, which are also equal to the doubled d_{SF} values.

Based on $\Delta E_{\mathrm{f}}(q)$ in the infinite limit $L \to \infty$ $[\Delta E_{\mathrm{f}}^{\mathrm{c}}(q)]$, reconstruction energies ΔE_{rec} were evaluated as follows:

$$\Delta E_{\mathrm{rec}} = \Delta E_{\mathrm{f}}^{\mathrm{c}}(\text{reconstructed}, q) - \Delta E_{\mathrm{f}}^{\mathrm{c}}(\text{unreconstructed}, q). \quad (6)$$

$\Delta E_{\mathrm{f}}^{\mathrm{c}}$(reconstructed, q) and $\Delta E_{\mathrm{f}}^{\mathrm{c}}$(unreconstructed, q) are the ones for the dislocation cores with and without DP reconstruction, respectively. This corresponds to energy gains due to atomic reconstructions at the dislocation cores. More negative ΔE_{rec} values indicate more stable states of the partial dislocations by reconstruction.

In the present calculations, it was also found that when excess electrons are present in a dislocation supercell (i.e., $q < 0$), they are essentially localized only at the cation core, as will be explained in Sec. III A. By contrast, when excess holes are introduced in a dislocation supercell (i.e., $q > 0$), they are localized just at the anion core. Although the present dislocation supercells always contain a pair of partial dislocations with a cation core and an anion core, therefore, the most stable atomic structures and their charge states of the cation and anion cores can be determined individually from calculations of the dislocation supercells [7].

III. RESULTS AND DISCUSSION

A. Dislocation core structures without excess carriers

Figures 3(a) and 3(b) shows the most stable atomic structures of the pristine partial dislocations without excess carriers (with $q = 0$) in ZnSe. It is found that the unreconstructed structures are more stable than DP-reconstructed structures. This is also the case with the partial dislocations in ZnS [7] and ZnTe (see Fig. S2 in the Supplemental Material [27]).

As reported previously, the pristine 30° partial dislocations in Si and GaAs have the DP reconstructed atomic structures as the energetically most stable structure [8,34,37]. In order

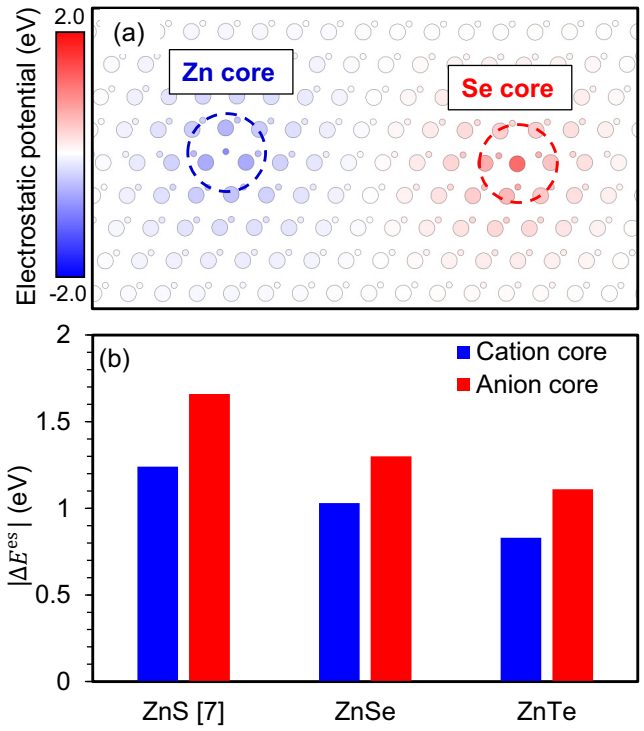

FIG. 4. (a) Excess electrostatic potentials at the atomic sites centered at the partial dislocation cores with respect to those in bulk. The atomic structures are viewed normal to the $(\bar{1}10)$ planes. (b) Absolute values of the excess electrostatic potentials at the partial-dislocation cores in the different crystal systems.

to understand such a difference in the dislocation-core structures, Fig. 4(a) displays electrostatic potentials at atomic sites around the pristine 30° partial dislocations in ZnSe with reference to those in the bulklike region (far from the dislocation cores). It can be seen that negative (positive) electrostatic potentials are localized at the Zn (Se) core. This can be understood in terms of partial ionicity of ZnSe. Owing to electronegativity differences of constituent elements, II-VI semiconductor crystals should contain partial ionicity in their chemical bonds. Moreover, the 30° partial dislocations have extra half planes, and thus include local off-stoichiometry at the cores. These factors can induce excess electrostatic potentials around the dislocation cores. In fact, absolute values of excess electrostatic potentials at the undercoordinated atomic sites centered at the dislocation cores ($|\Delta E^{es}|$) tend to decrease in the order of ZnS > ZnSe > ZnTe [see Fig. 4(b)]. This well agrees with the electronegativity-difference trend in these crystals. Larger ionicity of ZnS, ZnSe, and ZnTe makes formation of like-ion bonds needed for DP reconstruction [see Figs. 3(c) and 3(d)] energetically unfavorable.

Figure 5 shows LDOS curves of the unreconstructed partial dislocations with $q = 0$ in ZnSe, along with those in the bulklike region. The profiles for the dislocation cores are taken from the undercoordinated atoms at the dislocation-core centers and their nearest neighbors [the atoms circled in Figs. 3(a) and 3(b)]. By the presence of excess positive and negative electrostatic fields localized at the dislocation cores [see Fig. 4(a)], the LDOS profile of the Zn (Se) core tends to shift downward (upward) in energy, as compared to those in bulk, similar to the illustration in Fig. 2(a). Moreover,

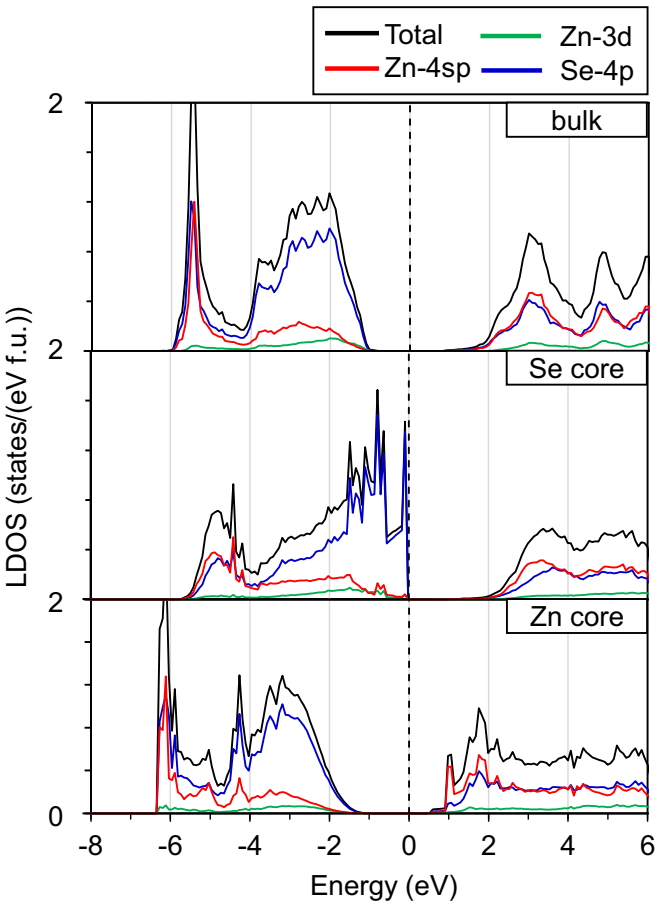

FIG. 5. LDOS curves for bulk ZnSe and the unreconstructed partial-dislocation cores with $q = 0$. The LDOS for bulk is taken from the atoms far from the dislocation cores. The LDOS curves for the dislocation cores are obtained from those for the central atoms at the dislocation cores and their nearest neighbors. The dashed line represents the highest occupied energy level.

local band gaps of the LDOS profiles at the dislocation cores become smaller than the band gap in bulk. This is because the Zn core forms the unoccupied defect level below the CBM in bulk, which originates from the $4s$ and $4p$ orbitals of Zn. Similarly, the Se core forms the fully occupied defect level above the VBM in bulk, which is mainly formed by the $4p$ orbitals of Se. These characteristic electronic structures of the dislocation cores may be closely related to interactions with carriers of electrons and holes excited by external light, which will be discussed below.

B. Dislocation core structures with excess carriers

As stated above, the pristine 30° partial dislocations with $q = 0$ in ZnS, ZnSe, and ZnTe tend to have the unreconstructed atomic structures at the cores. Since the dislocation cores have excess electrostatic potentials, it is expected that the partial dislocations may have attractive interactions with excess carriers of electrons and holes. This can be realized because such carriers can be excited by light illumination in these crystals. In this section, therefore, formation energies of the 30° partial dislocations in the presence of excess electrons

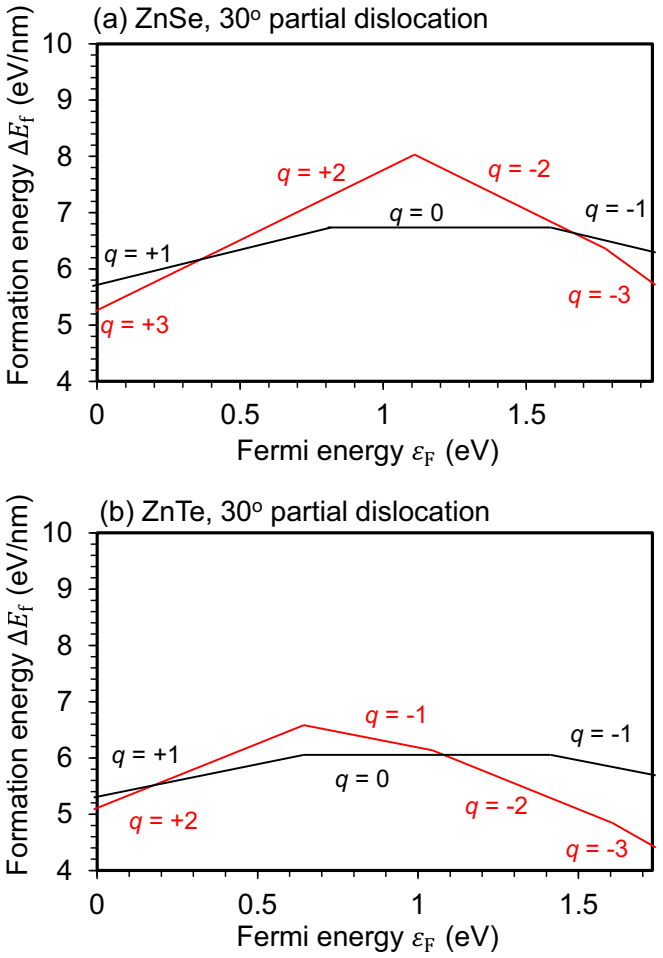

FIG. 6. Formation energies $\Delta E_f(q)$ as a function of the Fermi level ε_F for (a) ZnSe and (b) ZnTe, obtained from the 288-atom and 576-atom supercells. $\Delta E_f(q)$ for the unreconstructed and reconstructed DP structures are plotted by the black and red lines, respectively. Only the results with the most stable charge states are shown at respective ε_F.

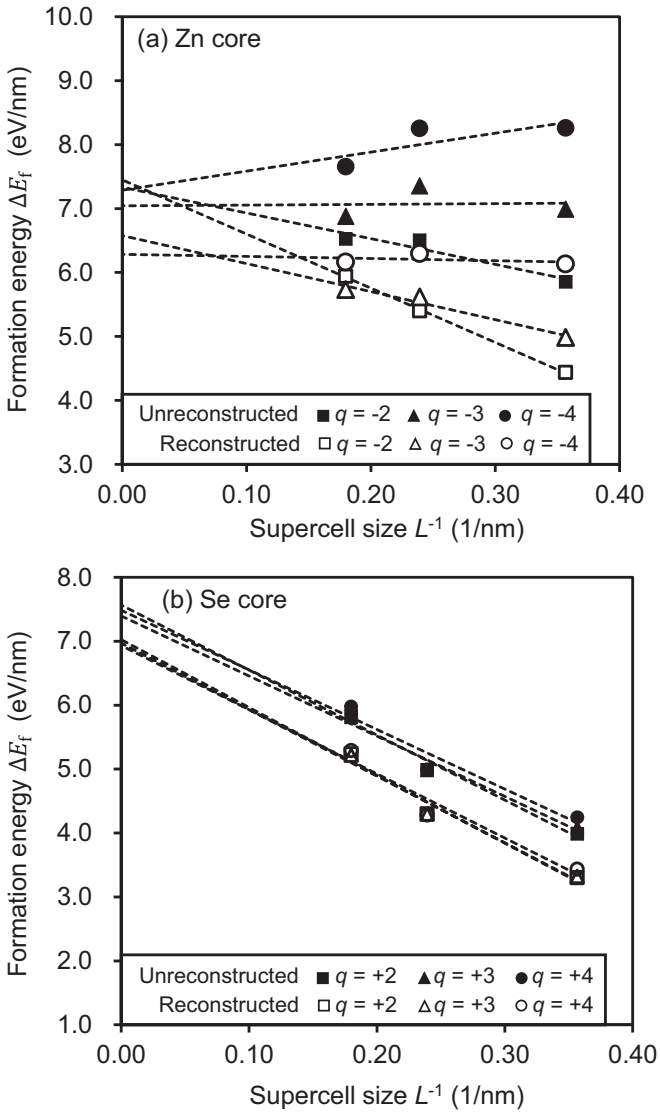

FIG. 7. Supercell-size dependence of $\Delta E_f(q)$ for the cation and anion cores in ZnSe.

and holes are evaluated, and the energetically most stable atomic structures at the cores are investigated.

Figure 6 shows calculated formation energies of the 30° partial dislocations with charge q [$\Delta E_f(q)$] as a function of ε_F. These results are obtained from the 288-atom (576-atom for DP reconstruction) supercells. In this figure, only the most stable charge states q against ε_F are displayed. It can be seen that the partial dislocations with charge q ($\neq 0$) can be more stable than the neutral ones ($q = 0$) when ε_F is around VBM or CBM. Moreover, relative stability of the unreconstructed and DP reconstructed atomic structures can be varied depending on ε_F. This is especially true when ε_F is located close to the VBM and the CBM.

Here the position of ε_F is noted. Since the present study assumes the semiconductor crystals without any dopants, the overall ε_F position is located in the middle of their band gaps. However, when electron-hole pairs are excited across the band gaps by external light and the electrons and holes are trapped at the cation or anion dislocation cores separately, ε_F positions at the dislocation cores are no longer present in the middle of the band gaps but lie close to the CBM for the cation cores and the VBM for the anion cores. This was described in more detail in our previous paper [7]. Therefore, it is worth paying attention to the formation energies at ε_F close to the CBM for the cation cores and the VBM for the anion cores.

The formation energies of the charged partial dislocations may be affected by the supercell size L. Figure 7 displays the formation energies $\Delta E_f(q)$ at $\varepsilon_F =$ the CBM for the cation cores and at $\varepsilon_F =$ the VBM for the anion cores in ZnSe as a function of the inverse supercell size L^{-1}, which are obtained from the different sized supercells. The results for ZnS and ZnTe are also shown in Figs. S3 and S4 in the Supplemental Material [27]. The L^{-1} dependencies are different for the atomic structures and species of the cores and the charge states. It is worth mentioning here that, for instance, the most stable charge state of the cation core in ZnSe in the limit of $L^{-1} = 0$ is -4 for the reconstructed structure, which is different from -3 in the 576-atom supercell (see Fig. 6).

Figures 3(c) and 3(d) display the atomic structures of the partial dislocations in the most stable charge states ($q = \pm 4$)

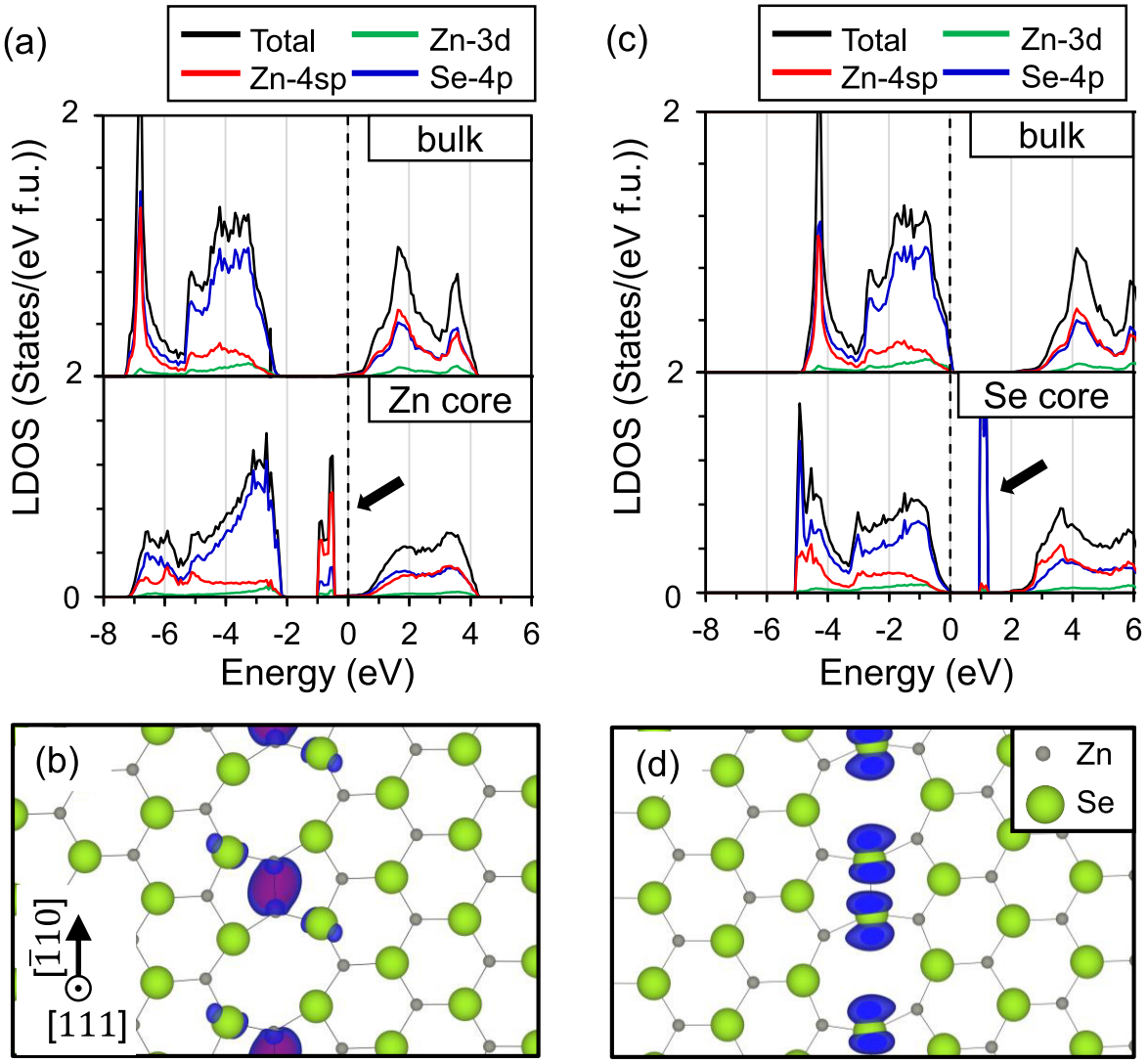

FIG. 8. LDOS curves of ZnSe for (a) the Zn core with $q = -4$ and (c) the Se core with $q = +4$. Band-decomposed charge densities of the defect-induced levels appearing within the band gap for (b) the Zn core and (d) the Se core.

in ZnSe (those in ZnTe are also displayed in Fig. S5 [27]). It can be seen that like atoms come close to each other along the dislocation lines in the presence of excess electrons or holes, resulting in DP reconstruction. The corresponding LDOS curves are also plotted in Fig. 8. It is clear that the reconstructed partial dislocations with the Zn and Se cores exhibit the extra levels localized around the middle of the band gap. The defect-induced levels of the Zn core are occupied by extra electrons while those at the Se core are unoccupied. Since the wave functions of the defect-induced levels are spatially localized at the reconstructed Zn and Se atoms of the cores [see Figs. 8(b) and 8(d)], these characteristic electronic structures originate from the fact that the Zn core traps extra electrons and the Se core captures extra holes. That is, localization of excess electrons and holes facilitate formation of like-ion bonds in the DP reconstructed structures [7]. Table II shows the reconstruction energies $\Delta E_{\rm rec}$ and the most stable charge states for the partial dislocations in the three different systems. Comparisons between $\Delta E_{\rm rec}$ of the anion cores among ZnS, ZnSe, and ZnTe show that $|\Delta E_{\rm rec}|$ values for the anion cores decrease as the atomic numbers of the anion increase. In contrast, $|\Delta E_{\rm rec}|$ values for the cation cores vary depending on the different crystals and show that ZnSe has smaller $|\Delta E_{\rm rec}|$ than ZnS and ZnTe. These trends cannot be simply explained by ionicity alone, indicating the importance of detailed electronic structures of the reconstructed partial-dislocation cores.

TABLE II. Most stable charge states q, core structures, and reconstruction energies $\Delta E_{\rm rec}$ obtained from the dislocation formation energies at $\varepsilon_{\rm F}$ = CBM for the cation cores and $\varepsilon_{\rm F}$ = VBM for the anion cores.

	Compound	q	Structure	$\Delta E_{\rm rec}$ (eV/nm)
Cationcore	ZnS	−4	DP	−1.37
	ZnSe	−4	DP	−1.01
	ZnTe	−4	DP	−1.33
Anioncore	ZnS	+3	DP	−0.83
	ZnSe	+4	DP	−0.55
	ZnTe	+2	DP	−0.24

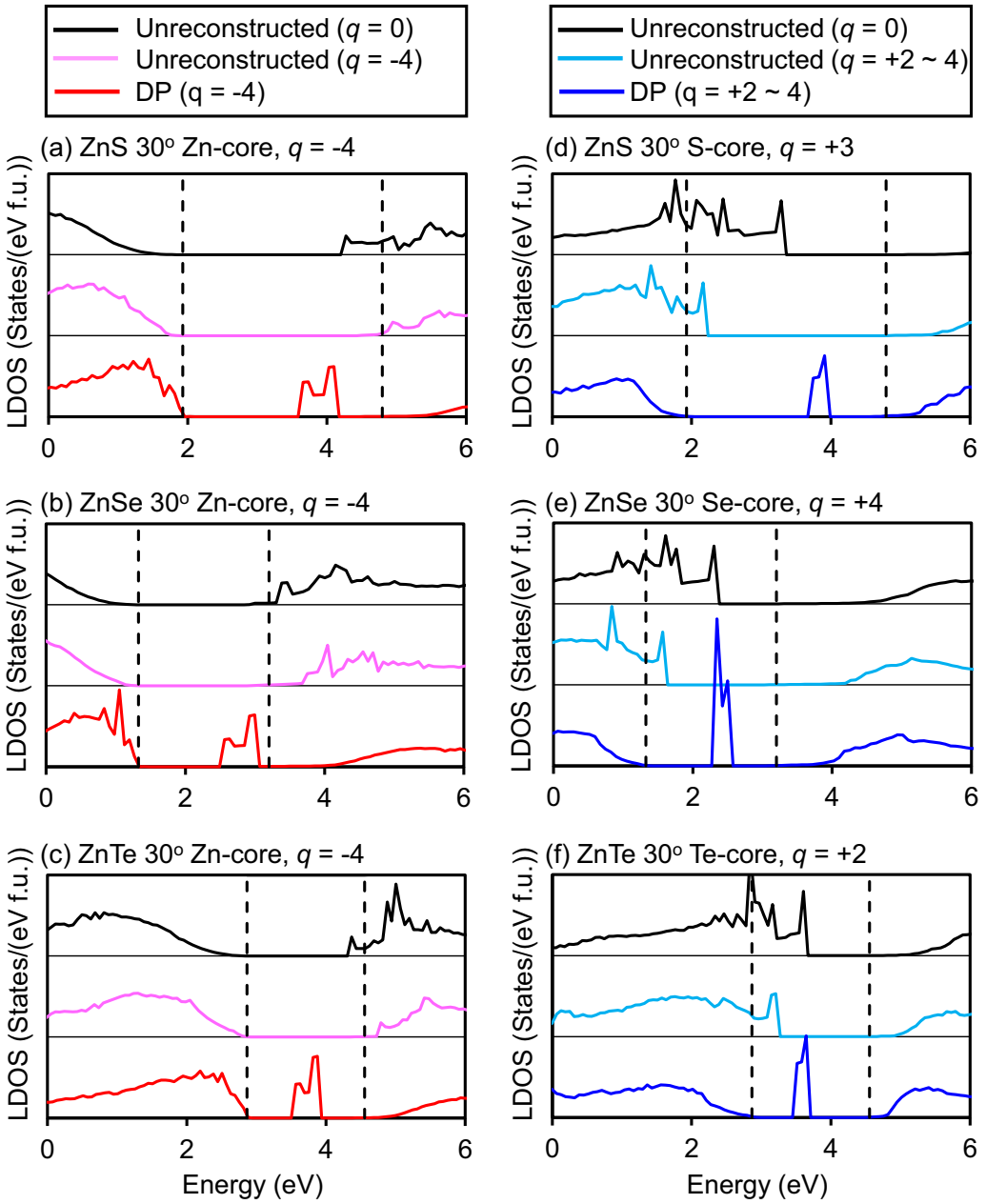

FIG. 9. LDOS curves for the charged unreconstructed and the charged reconstructed structures at the partial-dislocation cores in ZnS, ZnSe, and ZnTe. Bulk VBM and CBM positions in these crystals are indicated as black dashed lines. The charges q correspond to the ones in the most stable states in the infinite limit of the supercell size $L \to \infty$. LDOS curves for the neutral unreconstructed partial dislocations are also plotted for comparison.

C. Trend in $\Delta E_{\rm rec}$ of cation and anion cores

In order to understand the trends in $\Delta E_{\rm rec}$, LDOS profiles of the unreconstructed and reconstructed partial dislocations are investigated in more detail. Figure 9 displays LDOS curves of the cation cores for ZnS, ZnSe, and ZnTe in the most stable charge states in the infinite limit of the supercell size (see Fig. 7). Those of the neutral unreconstructed partial dislocations are also plotted as references. To facilitate direct comparisons among the LDOS curves for the different supercells, the band alignment is performed with respect to 1s orbital energies of Zn in the perfect crystal and in the region far from the dislocations in the supercells [38,39].

Regarding the cation cores [Figs. 9(a)–9(c)], the LDOS curves of the unreconstructed cores with $q \neq 0$ are shifted upward in energy by electrons trapping ($q = -4$), as compared to those for $q = 0$, so that the CBM positions are located close to that in bulk [see pink curves in Figs. 9(a)–9(c)]. On the other hand, extra levels of the reconstructed DP cores are produced in the band gaps and are mainly composed of the outermost sp orbitals of Zn at the cores, which can be referred to as defect-induced donorlike levels (see also Fig. 8). In this case, the trapped electrons at the defect levels are more stable with decreasing their energy positions from the CBM in bulk. Here, $E_{\rm dl}^{\rm cation}$ is defined as the values taken from the average energies of the defect levels of the reconstructed cores,

measured from the CBM in bulk. The $E_{\rm dl}^{\rm cation}$ values for ZnS, ZnSe, and ZnTe estimated from the LDOSs in Figs. 9(a)–9(c) are 0.91, 0.42, and 0.83, respectively. This trend agrees well with the one in $\Delta E_{\rm rec}$. The $E_{\rm dl}^{\rm cation}$ of ZnSe smaller than those of ZnS and ZnTe may originate from their energetic positions of the CBM in bulk. As can be seen in Fig. 9, the CBM position of bulk ZnSe determined by the band alignment is by approximately 1.5 eV lower than those of ZnS and ZnTe. This fact can also be confirmed by the previous hybrid-functional and *GW* calculations [18]. Such a lower CBM position of ZnSe may be related to the shallower donorlike defect level in ZnSe.

For the anion cores [Figs. 9(d)–9(f)], the LDOS curves of the charged unreconstructed cores are shifted downward in energy by hole trapping ($q = +2 \sim +4$). However, the VBM positions of the LDOS curves remain in the band gaps even after trapping holes for all three anion cores [see light blue curves in Figs. 9(d)–9(f)]. For the reconstructed cores, the explicit defect levels are produced in the band gaps and are mainly composed of the outermost p orbitals of the anions, which can be referred to as defect-induced acceptorlike levels (see also Fig. 8). It is generally known that holes in semiconductor crystals are more stabilized when their energy levels increase more within their band gaps. Therefore, energetic positions of the defect-induced levels $E_{\rm dl}^{\rm anion}$ are evaluated from the average energies of the defect levels of the reconstructed cores with respect to the VBM in bulk. $E_{\rm dl}^{\rm anion}$ values for ZnS, ZnSe, and ZnTe estimated from the LDOSs are 1.90, 1.10, and 0.71, respectively, whose trends also well agree with the one in $\Delta E_{\rm rec}$. In addition, since the reconstructed atomic structures at the anion cores accompany formation of like-ion bonds along the dislocation lines, the positions of the defect-induced acceptorlike levels may also be related to bonding interactions between the anions. In fact, bond dissociation energies of diatomic molecules S_2, Se_2, and Te_2 are 4.41, 3.43, and 2.67 eV, respectively [40], whose trend is in good agreement with that in $\Delta E_{\rm rec}$. In the molecular-orbital picture, stronger interactions between anions increase energies of their antibonding orbitals more, which may correspond to the defect-induced level positions.

D. Discussion

Finally, this section discusses the influence of the core reconstruction induced by carrier trapping on plastic deformation of crystals. When dislocations are about to move, they have to overcome the Peierls-potential barriers. The higher their Peierls-potential barriers, the lower the dislocation mobility. For the 30° unreconstructed partial-dislocation cores in ZnS, Hang *et al.* [41] estimated the heights of the Peierls-potential barriers by calculating the total-energy differences between the unreconstructed structure and its metastable structure (Fig. S6 [27]), which was assumed to appear during the dislocation glide. Their estimated Peierls-potential barrier height was 0.4 and 0.3 eV/nm for the Zn and S cores, respectively. It is also confirmed from our similar test calculations for ZnSe (288-atom supercells) that Peierls-potential barriers are 0.5 and 0.1 eV/nm for the Zn and Se cores, respectively. It is considered that these values correspond to the Peierls-potential barrier heights for the glide partial dislocations without carrier trapping, namely, without light illumination. When the partial dislocations undergo DP reconstruction due to carrier trapping (under light illumination) and start to glide, the reconstructed like-ion bonds should be broken. This is because the periodic atomic arrangements of the host crystals have to be maintained after the partial-dislocation glide. Since such bond breaking at the reconstructed partial-dislocation cores requires more energy expenses upon glide, it is thus most likely that $\Delta E_{\rm rec}$ contributes to increasing the Peierls-potential barriers in ZnS, ZnSe, and ZnTe. It is worth claiming that the absolute values of $\Delta E_{\rm rec}$ in Table II tend to be comparable to or larger than the Peierls-potential barrier heights estimated for the unreconstructed partial dislocations as mentioned above. Since the $\Delta E_{\rm rec}$ values lead to decreasing potential energies of the partial dislocations at their stationary points, it is expected that the heights of Peierls-potential barriers of the reconstructed dislocations in turn become at most several times higher than those of the unreconstructed ones. Such increases in Peierls potential barrier should result in significant suppression of the dislocation mobility in ZnSe and ZnTe as well as ZnS. This can reasonably explain the experimentally observed hardening of the Zn compounds by light illumination.

IV. CONCLUSIONS

Most stable atomic structures and the carrier-trapping effects of partial dislocations in ZnSe and ZnTe were investigated by GGA + U calculations, along with the results in ZnS. Among possible partial dislocations in the zincblende structure, as a typical example, 30° partial dislocations with the cation and anion cores were selected. It was found that the partial dislocations in these crystals tend to have unreconstructed atomic structures at their cores in the absence of excess carriers. It was also confirmed that the partial dislocations possess excess electrostatic potentials at their cores, which is due to ionicity of the host crystals and can facilitate interactions with excited carriers by light illumination. In contrast, formation energies of the partial dislocations with/without excess carriers were evaluated, and it was found that atomic reconstructions at the cation (anion) cores energetically favorably take place by the trapping of excess electrons (holes). It is thought that the reconstruction energies $|\Delta E_{\rm rec}|$ should contribute to increasing the Peierls-potential barrier heights, resulting in the decreased dislocation mobility, namely, hardening of the crystals. The $|\Delta E_{\rm rec}|$ values at the anion cores decreased more with increasing atomic numbers of the anions (ZnS > ZnSe > ZnTe), while for the Zn cores, $|\Delta E_{\rm rec}|$ at the Zn core in ZnSe shows lower value than those in ZnS and ZnTe. From analyses of LDOS curves, the above trends in $|\Delta E_{\rm rec}|$ can be explained by energetic positions of the defect-induced levels trapping carriers within the band gaps.

ACKNOWLEDGMENTS

This work was supported by JSPS KAKENHI (Grants No. JP19H05786 and No. JP21H04618), JST-CREST (Grant No. JPMJCR17J1), and "Nagoya University Interdisciplinary Frontier Fellowship" supported by JST and Nagoya University.

[1] C. N. Ahlquist, M. J. Carroll, and P. Stroempl, The photoplastic effect in wurtzite and sphalerite structure II-VI compounds, J. Phys. Chem. Solids **33**, 337 (1972).

[2] Y. A. Osip'yan, V. F. Petrenko, A. V. Zaretskiĭ, and R. W. Whitworth, Properties of II–VI semiconductors associated with moving dislocations, Adv. Phys. **35**, 115 (1986).

[3] K. Nakagawa, K. Maeda, and S. Takeuchi, Plastic deformation of CdTe single crystals II. Photoplastic effect of II-VI compounds, J. Phys. Soc. Jpn. **50**, 3040 (1981).

[4] Y. Oshima, A. Nakamura, and K. Matsunaga, Extraordinary plasticity of an inorganic semiconductor in darkness, Science (80-.) **360**, 772 (2018).

[5] K. Matsunaga, M. Yoshiya, N. Shibata, H. Ohta, and T. Mizoguchi, Ceramic science of crystal defect cores, J. Ceram. Soc. Jpn. **130**, 648 (2022).

[6] A. Nakamura, X. Fang, A. Matsubara, E. Tochigi, Y. Oshima, T. Saito, T. Yokoi, Y. Ikuhara, and K. Matsunaga, Photoindentation: A new route to understanding dislocation behavior in light, Nano Lett. **21**, 1962 (2021).

[7] K. Matsunaga, S. Hoshino, M. Ukita, Y. Oshima, T. Yokoi, and A. Nakamura, Carrier-Trapping induced reconstruction of partial-dislocation cores responsible for light-illumination controlled plasticity in an inorganic semiconductor, Acta Mater. **195**, 645 (2020).

[8] M. M. De Araújo, J. F. Justo, and R. W. Nunes, Electronic charge effects on dislocation cores in silicon, Appl. Phys. Lett. **85**, 5610 (2004).

[9] K. Maeda and S. Takeuchi, Enhanced glide of dislocations in GaAs single crystals by electron beam irradiation, Jpn. J. Appl. Phys. **20**, L165 (1981).

[10] K. Maeda and S. Takeuchi, Recombination enhanced mobility of dislocations in III-V compounds, J. Phys. Colloq. (Paris) **44**, 375 (1983).

[11] K. Maeda and S. Takeuchi, Recombination enhanced dislocation glide in InP single crystals, Appl. Phys. Lett. **42**, 664 (1983).

[12] P. E. Blöchl, Projector augmented-wave method, Phys. Rev. B **50**, 17953 (1994).

[13] G. Kresse and J. Hafner, *Ab initio* molecular dynamics for open-shell transition metals, Phys. Rev. B **48**, 13115 (1993).

[14] J. P. Perdew, K. Burke, and M. Ernzerhof, Generalized Gradient Approximation Made Simple, Phys. Rev. Lett. **77**, 3865 (1996).

[15] S. Z. Karazhanov, P. Ravindran, A. Kjekshus, H. Fjellvåg, U. Grossner, and B. G. Svensson, Coulomb correlation effects in zinc monochalcogenides, J. Appl. Phys. **100**, 043709 (2006).

[16] L. Ley, R. A. Pollak, F. R. McFeely, S. P. Kowalczyk, and D. A. Shirley, Total valence-band densities of states of III-V and II-VI compounds from X-Ray photoemission spectroscopy, Phys. Rev. B **9**, 600 (1974).

[17] C. W. Zhang, C. Han, S. S. Yan, and F. B. Zheng, Design of ferromagnetism in Cu-doped ZnO Nanowires: First-principles prediction, Europhys. Lett. **95**, 47011 (2011).

[18] M. S. Khan, L. Shi, and B. Zou, Impact of vacancy defects on optoelectronic and magnetic properties of Mn-doped ZnSe, Comput. Mater. Sci. **174**, 109493 (2020).

[19] H. H. Pham, G. T. Barkema, and L. W. Wang, DFT + U studies of Cu doping and p-type compensation in crystalline and amorphous ZnS, Phys. Chem. Chem. Phys. **17**, 26270 (2015).

[20] Y. Hinuma, A. Grüneis, G. Kresse, and F. Oba, Band alignment of semiconductors from density-functional theory and many-body perturbation theory, Phys. Rev. B **90**, 155405 (2014).

[21] S. Takeuchi and K. Suzuki, Stacking fault energies of, tetrahedrally coordinated crystals, Phys. Status Solidi Appl. Res. **171**, 99 (1999).

[22] G. Rivaud, and J. C. Desoyer, Plastic deformation of II-VI compounds with sphalerite structure: Example ZnSe, ZnTe, J. Phys. Colloq. (Paris) **44**, 387 (1983).

[23] S. Takeuchi, K. Suzuki, K. Maeda, and H. Iwanaga, Stacking-fault energy of II–VI compounds, Philos. Mag. A **50**, 171 (1985).

[24] G. Lu and D. J. H. Cockayne, Partial separations of extended α and β dislocations in II–VI semiconductors, Philos. Mag. A **53**, 307 (1986).

[25] M. Ukita, R. Nagahara, Y. Oshima, A. Nakamura, T. Yokoi, and K. Matsunaga, Theoretical calculations of characters and stability of glide dislocations in zinc sulfide, Mater. Trans. **60**, 99 (2019).

[26] M. Peach and J. S. Koehler, The forces exerted on dislocations and the stress fields produced by them, Phys. Rev. **80**, 436 (1950).

[27] See Supplemental Material at http://link.aps.org/supplemental/10.1103/PhysRevMaterials.7.013603 for the cluster-model result, additional data on atomic structures of the dislocation cores, and the formation-energy analyses.

[28] J. Bennetto, J. W. Nunes, and D. Vanderbilt, Period-Doubled Structure for the 90° Partial Dislocation in Silicon, Phys. Rev. Lett. **79**, 245 (1997).

[29] J. F. Justo, V. V. Bulatov, and S. Yip, Dislocation core reconstruction and its effect on dislocation mobility in silicon, J. Appl. Phys. **86**, 4249 (1999).

[30] X. Blase, K. Lin, A. Canning, S. G. Louie, and D. C. Chrzan, Structure and Energy of the 90° Partial Dislocation in Diamond: A Combined *Ab Initio* and Elasticity Theory Analysis, Phys. Rev. Lett. **84**, 5780 (2000).

[31] R. W. Nunes and D. Vanderbilt, Models of core reconstruction for the 90° partial dislocation in semiconductors, J. Phys.: Condens. Matter **12**, 10021 (2000).

[32] A. T. Blumenau, R. Jones, and T. Frauenheim, The 60° dislocation in diamond and its dissociation, J. Phys.: Condens. Matter **15**, S2951 (2003).

[33] G. Savini, A. T. Blumenau, M. I. Heggie, and S. Öberg, Structure and energy of partial dislocations in wurtzite-GaN, Phys. Status Solidi (c) **4**, 2945 (2007).

[34] J. S. Park, B. Huang, S. H. Wei, J. Kang, and W. E. McMahon, Period-Doubling reconstructions of semiconductor partial dislocations, NPG Asia Mater. **7**, e216 (2015).

[35] A. García and J. E. Northrup, Compensation of P-Type Doping in ZnSe: The Role of Impurity-Native Defect Complexes, Phys. Rev. Lett. **74**, 1131 (1995).

[36] G. Makov and M. C. Payne, Periodic boundary conditions in *ab initio* calculations, Phys. Rev. B **51**, 4014 (1995).

[37] R. Nunes, J. Bennetto, and D. Vanderbilt, Atomic structure of dislocation kinks in silicon, Phys. Rev. B **57**, 10388 (1998).

[38] C. Li, Y. Wu, T. J. Pennycook, A. R. Lupini, D. N. Leonard, W. Yin, N. Paudel, M. Al-Jassim, Y. Yan, and S. J. Pennycook, Carrier Separation at Dislocation Pairs in CdTe, Phys. Rev. Lett. **111**, 096403 (2013).

[39] J. Wei, T. Ogawa, B. Feng, T. Yokoi, R. Ishikawa, A. Kuwabara, K. Matsunaga, N. Shibata, and Y. Ikuhara, Direct measurement of electronic band structures at oxide grain boundaries, Nano Lett. **20**, 2530 (2020).

[40] Y. R. Luo, *Comprehensive Handbook of Chemical Bond Energies* (CRC, Boca Raton, FL, 2007).

[41] L. Huang and S. Wang, A theoretical investigation of the glide dislocations in the sphalerite ZnS, J. Appl. Phys. **124**, 175702 (2018).